


Combined Coulombic and magnetic contributions to dispersion in $e + {}^{12}\text{C}$ collisionsD. H. Jakubassa-Amundsen *Mathematics Institute, University of Munich, Theresienstrasse 39, 80333 Munich, Germany*

(Received 2 February 2022; accepted 18 March 2022; published 9 May 2022)

Dispersion corrections to elastic electron scattering from a ${}^{12}\text{C}$ nucleus are calculated within the second-order Born approximation. Three strong transient nuclear excitations are considered, at 4.439 MeV (2^+), 17.7 MeV (1^-), and 23.5 MeV (1^-). The Friar-Rosen-type Coulomb term is supplemented with the transverse part of the photon propagator. It is found that the dispersive cross-section changes in the first diffraction minimum reach nearly 10%, rising more slowly with collision energy beyond 400 MeV. Magnetic scattering can be strong for the individual excited states and lowers the dispersion effect considerably at energies below 400 MeV. However, it contributes at most 10% at the higher energies investigated.

DOI: [10.1103/PhysRevC.105.054303](https://doi.org/10.1103/PhysRevC.105.054303)**I. INTRODUCTION**

The discrepancies between the quantum-electrodynamical (QED) corrected elastic scattering data in the vicinity of the first diffraction minimum of the differential cross section [1–4] and calculations based on the phase-shift approximation are still outstanding problems [5]. These deviations are commonly attributed to the virtual excitation of the target nucleus during the scattering process, known as dispersion. Such effects were first investigated by Schiff [6] and by Lewis [7], using a closure approximation for evaluating the sum over the transient nuclear excitations, together with simple parametrizations of the nuclear charge distributions and correlation functions.

A more advanced treatment of the dispersion effects, particularly for the ${}^{12}\text{C}$ nucleus, was provided by Friar and Rosen [8,9]. They also used the closure approximation, which was subsequently improved by some correction terms. However, they employed a harmonic-oscillator-based model for the resulting ground-state correlation function. There were further dispersion estimates for ${}^{12}\text{C}$ at 50-MeV impact by Bottino and Ciocchetti [10], who avoided the closure approximation and instead described the transition to excited states in terms of approximate form factors. De Forest [11] considered explicitly all nuclear excited states up to the tenth shell, calculated within the harmonic-oscillator model, but used an ${}^{16}\text{O}$ target. All these papers considered only the Coulombic contribution in the photon propagators, responsible for the charge-charge interaction between the impinging electron and the target nucleus, in order to account for the dominant contribution.

Magnetic dispersion corrections were investigated by Goldberg [12] in the case of a helium target. He also made the closure approximation and treated the helium nucleons as independent particles, thus ignoring correlation effects. Moreover, for coping with the integrals, he made an expansion which is only valid for the backmost scattering angles. By

considering only one of the transverse terms and only the convection current, he estimated the magnetic contribution to elastic scattering to be well below 1%, i.e., much smaller than the Coulombic contribution to dispersion.

A reinvestigation of magnetic scattering is motivated by the fact that in nuclear excitation, magnetic contributions can play a role even in the forward hemisphere [13]. Transverse transitions are particularly important for the excitation of the giant-dipole resonance [14,15], which extends in ${}^{12}\text{C}$ from 15 to 35 MeV [16]. Such excitations are described by using transition densities calculated within the quasiparticle random-phase approximation (QRPA) or with the more elaborate quasiparticle-phonon model (QPM) [17,18]. These densities consider both convection and magnetization currents, as well as the correlation between the nucleons.

In the present work all transverse parts of the photon propagator, which are allowed by the requirement of gauge invariance [12], are retained. Moreover, instead of employing the closure approximation, the virtual excitation of two strong high-energy dipole and one quadrupole state is explicitly considered. This choice is based on investigations where giant-dipole intermediate states, constructed from particle-hole harmonic-oscillator basis states, were taken into account [19]. We were also inspired by the prediction [10] that excitations of low multipolarity, in particular, dipole, will provide the dominant contribution to dispersion for collision energies well below 1 GeV. And finally, it was discovered in spin-asymmetry considerations that highly excited states are extremely important for the dispersion effect [20,21].

The paper is organized as follows. In Sec. II the theory is outlined, and Sec. III provides some numerical ingredients. Results for the dispersion correction at collision energies from 220 to 750 MeV are given in Sec. IV, followed by the conclusion (Sec. V). Atomic units ($\hbar = m = e = 1$) are used unless indicated otherwise.

II. THEORY

The exchange of two photons, as occurs in dispersion, is described in terms of the Feynman box diagram [4,22]. Only the direct box graph will be considered here. Within the second-order Born approximation, the transition amplitude for dispersion is given by [9,23]

$$M_{fi} = \frac{4\pi}{(2\pi)^3} \left(\frac{e^2}{c}\right)^2 \int d\mathbf{p} \frac{1}{(q_2^2 + i\epsilon)(q_1^2 + i\epsilon)} \times \sum_{\mu,\nu=0}^3 t_{\mu\nu}(\omega_1) \sum_{n \neq 0} T_n^{\mu\nu}, \quad (2.1)$$

where $\omega_1 = E_i - \omega_n - \sqrt{(\mathbf{q}_1 c)^2 + M_T^2 c^4} + M_T c^2$ is the pole of the nuclear propagator. In this expression, E_i is the total energy of the impinging electron and M_T is the nuclear mass number. The contribution from the poles of the electron propagator, which enters into (2.1) in terms of

$$t_{\mu\nu}(\omega_1) = c u_{k_f}^{(\sigma_f)+} \gamma_0 \gamma_\mu \frac{\omega_1 + c\boldsymbol{\alpha}\mathbf{p} + \beta mc^2}{\omega_1^2 - \mathbf{p}^2 c^2 - m^2 c^4 + i\epsilon} \times \gamma_0 \gamma_\nu u_{k_i}^{(\sigma_i)}, \quad (2.2)$$

is neglected as being of minor importance [9]. Here, \mathbf{k}_i and \mathbf{k}_f are, respectively, the initial and final momenta of the electron, which is described by the free four-spinors $u_{k_i}^{(\sigma_i)}$ and $u_{k_f}^{(\sigma_f)}$ with spin projections σ_i and σ_f [24]. The symbols β , $\boldsymbol{\alpha}$, γ_0 , γ_ν denote Dirac matrices. The sum over n in (2.1) runs over all nuclear states with excitation energy $\omega_n \neq 0$, and $T_n^{\mu\nu}$ is the nuclear tensor component. The four-momenta q_1 and q_2 from the two photon propagators are interrelated with the intermediate electron momentum $p = (\omega_1/c, \mathbf{p})$ by $q_1 = k_i - p$ and $q_2 = p - k_f$.

Making use of the gauge invariance, one can decompose [9,12]

$$\frac{g^{\mu\nu}}{q^2 + i\epsilon} = -\frac{1}{q^2} \delta_{\mu 0} \delta_{\nu 0} - \frac{\delta_{mn} - \hat{q}^m \hat{q}^n}{q^2 + i\epsilon} \delta_{\mu m} \delta_{\nu n}, \quad (2.3)$$

where $g^{\mu\nu}$ is the metric tensor, $\mu = 0, m$ with $m = 1, 2, 3$ and $\hat{q}^m = q^m/|q|$. The first term refers to the Coulombic contribution, and the second term denotes the transverse part of the photon propagator. This leads to the decomposition, using $t_{\mu\nu} T_n^{\mu\nu} = t_{\mu\nu} \sum_{\rho\tau} g^{\mu\rho} g^{\nu\tau} T_{n,\rho\tau}$ [24]:

$$\begin{aligned} \sum_{\mu,\nu=0}^3 t_{\mu\nu} \frac{1}{(q_2^2 + i\epsilon)(q_1^2 + i\epsilon)} T_n^{\mu\nu} &= \frac{1}{q_1^2 q_2^2} t_{00} T_{n,00} \\ &+ \frac{1}{(q_1^2 + i\epsilon) q_2^2} \left[\sum_{m=1}^3 t_{0m} \left(T_{n,0m} - \hat{q}_1^m \sum_{k=1}^3 \hat{q}_1^k T_{n,0k} \right) \right] \\ &+ \frac{1}{q_1^2 (q_2^2 + i\epsilon)} \left[\sum_{m=1}^3 t_{m0} \left(T_{n,m0} - \hat{q}_2^m \sum_{k=1}^3 \hat{q}_2^k T_{n,k0} \right) \right] \\ &+ R_n. \end{aligned} \quad (2.4)$$

The fourth term, R_n , relates to the product of the two transverse parts:

$$R_n = \frac{1}{(q_1^2 + i\epsilon)(q_2^2 + i\epsilon)} \sum_{r,k=1}^3 \left(t_{rk} - \hat{q}_2^r \sum_{m=1}^3 \hat{q}_2^m t_{mk} \right) \times \left(T_{n,rk} - \hat{q}_1^k \sum_{i=1}^3 \hat{q}_1^i T_{n,ri} \right). \quad (2.5)$$

It is of opposite sign as compared to the first two transverse terms in (2.4) and will be of importance for nuclear excitations with a strong magnetic contribution.

The nuclear tensor component $T_{n,00}$ describes the excitation of the state $|n\rangle$ and the subsequent return to the ground state $|0\rangle$, mediated by the charge transition density ϱ :

$$T_{n,00} = \langle 0 | \varrho(\mathbf{q}_2) | n \rangle \langle n | \varrho(\mathbf{q}_1) | 0 \rangle, \quad n \neq 0. \quad (2.6)$$

Since ^{12}C is a spin-zero nucleus, only one multipole L contributes to the excitation of the state $|n\rangle$. Hence [25,26]

$$\begin{aligned} \langle n | \varrho(\mathbf{q}) | 0 \rangle &= \int d\mathbf{r}_N \varrho_{n0}(\mathbf{r}_N) e^{i\mathbf{q}\mathbf{r}_N} \\ &= \int d\mathbf{r}_N \varrho_L(\mathbf{r}_N) Y_{LM}^*(\hat{\mathbf{r}}_N) e^{i\mathbf{q}\mathbf{r}_N}, \end{aligned} \quad (2.7)$$

where $\varrho_L(\mathbf{r}_N)$ is the transition density in coordinate space, calculated from nuclear models (see, e.g., [27]), and Y_{LM} is a spherical harmonic function [28]. Equation (2.7) is readily expressed in terms of the charge form factor F_L^c ,

$$\langle n | \varrho(\mathbf{q}) | 0 \rangle = 4\pi i^L F_L^c(|\mathbf{q}|) Y_{LM}^*(\hat{\mathbf{q}}), \quad (2.8)$$

where $F_L^c(q) = \int r_N^2 dr_N \varrho_L(\mathbf{r}_N) j_L(qr_N)$ with j_L a spherical Bessel function [29].

The tensor components $T_{n,0m}$ and $T_{n,m0}$ refer to one transition induced by ϱ , the second one by the current transition density $\mathbf{J} = (J_m)_{m=1,2,3}$,

$$\begin{aligned} T_{n,m0} &= \langle 0 | J_m(\mathbf{q}_2) | n \rangle \langle n | \varrho(\mathbf{q}_1) | 0 \rangle, \\ T_{n,0m} &= \langle 0 | \varrho(\mathbf{q}_2) | n \rangle \langle n | J_m(\mathbf{q}_1) | 0 \rangle, \quad n \neq 0. \end{aligned} \quad (2.9)$$

The components $T_{n,rk}$ describe transitions where excitation and decay are due to the current transition density,

$$T_{n,rk} = \langle 0 | J_r(\mathbf{q}_2) | n \rangle \langle n | J_k(\mathbf{q}_1) | 0 \rangle. \quad (2.10)$$

Considering excited states with parity $(-1)^L$, the magnetic transition density in coordinate space is defined by [26,27,30]

$$\mathbf{J}_{n0}(\mathbf{r}_N) = -i \sum_{\lambda=L\pm 1} J_{L\lambda}(\mathbf{r}_N) \mathbf{Y}_{L\lambda}^{*M}(\hat{\mathbf{r}}_N), \quad (2.11)$$

where $\mathbf{Y}_{L\lambda}^{*M}$ is a vector spherical harmonics [28]. In Fourier space one gets

$$\begin{aligned} \langle n | \mathbf{J}(\mathbf{q}) | 0 \rangle &= \int d\mathbf{r}_N \mathbf{J}_{n0}(\mathbf{r}_N) e^{i\mathbf{q}\mathbf{r}_N} \\ &= -4\pi i \sum_{\lambda=L\pm 1} i^\lambda F_{L\lambda}^{te}(|\mathbf{q}|) \mathbf{Y}_{L\lambda}^{*M}(\hat{\mathbf{q}}), \end{aligned} \quad (2.12)$$

where the transverse form factor $F_{L\lambda}^{te}(q) = \int r_N^2 dr_N J_{L\lambda}(r_N) j_\lambda(qr_N)$ has been introduced. We note that the sum over n in (2.1) runs for a given angular momentum state L also over its magnetic quantum numbers M . Using completeness, this sum can easily be carried out in the case of $T_{n,00}$ [28],

$$\sum_{M=-L}^L T_{L,00} = 4\pi(2L+1)F_L^c(|\mathbf{q}_1|)F_L^c(|\mathbf{q}_2|)P_L(\cos\vartheta_{12}), \quad (2.13)$$

where P_L is a Legendre polynomial and ϑ_{12} is the angle between \mathbf{q}_1 and \mathbf{q}_2 .

The differential cross section for the elastic scattering of unpolarized electrons, including dispersion, is in lowest order given by [9,23]

$$\frac{d\sigma^{\text{box}}}{d\Omega_f} = \frac{|\mathbf{k}_f|}{|\mathbf{k}_i|} \frac{1}{f_{\text{rec}}} \frac{1}{2} \sum_{\sigma_i\sigma_f} [|f_{\text{coul}}|^2 + 2 \text{Re} \{ f_{\text{coul}}^* A_{fi}^{\text{box}} \}], \quad (2.14)$$

where A_{fi}^{box} comprises the four contributions according to (2.4)

$$A_{fi}^{\text{box}} = 2\sqrt{\frac{E_i E_f}{c^2}} \sum_L [M_{fi}^c(L) + M_{fi}^{te1}(L) + M_{fi}^{te2}(L) + M_{fi}^{te3}(L)], \quad (2.15)$$

and $f_{\text{coul}}(\sigma_i\sigma_f)$ is the Coulomb scattering amplitude, consisting of the direct term A and the spin-flip term B as calculated within the phase-shift analysis [31]. If $u_{k_i}^{(\sigma_i)}$ and $u_{k_f}^{(\sigma_f)}$ represent helicity eigenstates ($\sigma = +/ -$ for positive/negative helicity), one has

$$\begin{aligned} f_{\text{coul}}(++) &= f_{\text{coul}}(--)=A, \\ f_{\text{coul}}(+-) &= -f_{\text{coul}}(-+)=iB. \end{aligned} \quad (2.16)$$

Due to the small mass M_T of the light ^{12}C nucleus, the consideration of recoil is important, leading to a final (total) energy E_f which is smaller than E_i . In the first-order Born approximation for f_{coul} , where the inclusion of recoil is straightforward, it leads to a shift of the position of the first diffraction minimum of the Coulomb cross section to higher angles. In the phase-shift analysis used here, recoil is accounted for by using an average collision energy \bar{E} instead of $E_{i,\text{kin}}$ (where $E_{\text{kin}} = E - c^2$ is the kinetic energy),

$$\bar{E} = \sqrt{E_{i,\text{kin}} E_{f,\text{kin}}}, \quad (2.17)$$

adopting the prescription of [32,33]. The application of (2.17) is important, since only then does the calculated minimum position of the Coulomb cross section, $d\sigma^{\text{coul}}/d\Omega_f = (|A|^2 + |B|^2)|\mathbf{k}_f|/(|\mathbf{k}_i|f_{\text{rec}})$, agree with experiment. This is demonstrated in Fig. 1 for 431.4-MeV electron impact, in comparison with the experimental data. The increase of angle with recoil is clearly seen.

Figure 2(a) shows the position ϑ_{min} of the first cross-section minimum as a function of collision energy. The displayed data points were obtained by means of spline interpolating the measured angular distributions and subsequently selecting the angle which corresponds to their minimum

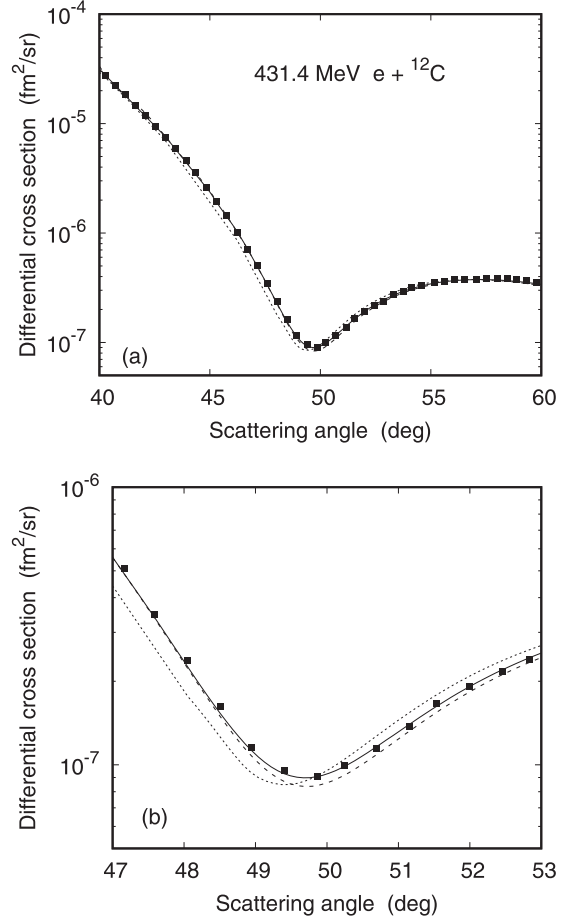


FIG. 1. (a) Elastic scattering cross section for 431.4-MeV $e + ^{12}\text{C}$ collisions as a function of scattering angle ϑ_f . Shown is $d\sigma_{\text{coul}}/d\Omega_f$ with (---) and without (.....) the consideration of recoil in comparison with the measurements of Offermann *et al.* [4]. Included is the total cross section $d\sigma^{\text{box}}/d\Omega_f$ from (2.14) with (2.15) (—). (b) is an enlarged version of (a).

cross-section value. The change of ϑ_{min} with respect to the no-recoil Coulombic result, both for theory and experiment, is explicitly depicted in Fig. 2(b). Also here, the consideration of recoil improves the agreement with the measurements. The additional recoil prefactor f_{rec} in (2.14) is given by [34]

$$f_{\text{rec}} = 1 - \frac{q^2 E_f}{2M_T c^2 k_f^2} \left(1 - \frac{c^2}{M_T E_f} \right), \quad (2.18)$$

with $q = k_i - k_f$ the momentum transfer.

Below the integrals inherent in the four contributions to (2.15) are provided, using the optimum choice of integration variables. For the Friar-Rosen-type term M_{fi}^c , corresponding to the Coulombic contribution in (2.4), the integration variable is shifted from \mathbf{p} to $\mathbf{p}' = \mathbf{p} - \mathbf{k}_i = -\mathbf{q}_1$ such that $\mathbf{q}_2 = \mathbf{p}' + \mathbf{q}$, and $\omega_1 = E_i - \omega_L - \sqrt{p'^2 c^2 + M_T^2 c^4} + M_T c^2$ becomes angle independent. Here and below the identification $p' \equiv |\mathbf{p}'|$, $T_{L,rk} \equiv T_{n,rk}$ and $\omega_L \equiv \omega_n$ is used. Then (setting $e = 1$),

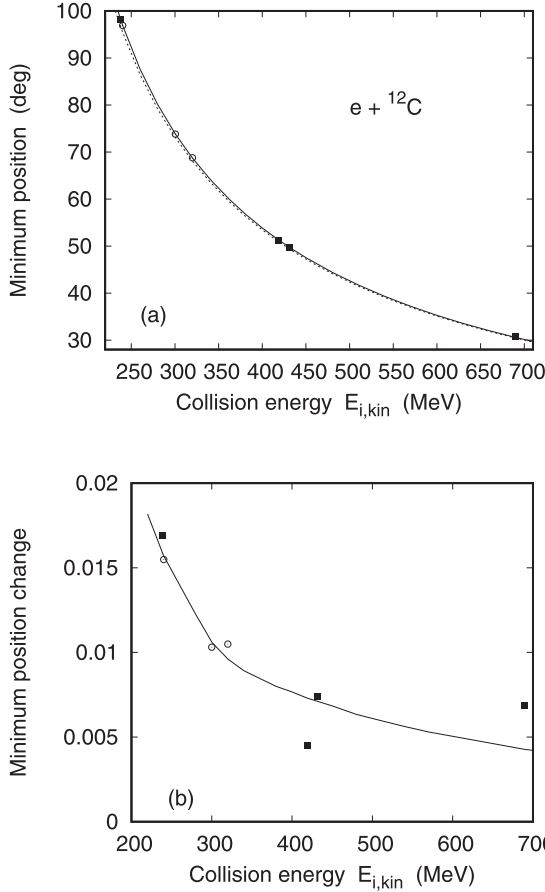


FIG. 2. (a) Position ϑ_{\min} of the first diffraction minimum as a function of collision energy $E_{i,\text{kin}}$. Shown are the results from the recoil-corrected (—) and no-recoil (⋯) phase-shift analysis. The experimental data are from Offermann and co-workers (■, [3,4]) and from Reuter *et al.* (○, [2]). For the datum point at 690 MeV, see text in Sec. IV B. (b) Angular change $\Delta\vartheta_{\min} = \vartheta_{\min}(\bar{E})/\vartheta_{\min}(E_{i,\text{kin}}) - 1$ as a function of collision energy in comparison with the respective experimental data points from (a).

$$M_{fi}^c(L) = \frac{2(2L+1)}{\pi c} \int_0^\infty dp' \int d\Omega_{p'} \frac{1}{(\mathbf{p}' + \mathbf{q})^2} \times \frac{u_{k_f}^{(\sigma_f)+} [\omega_1 + c\boldsymbol{\alpha}(\mathbf{p}' + \mathbf{k}_i) + \beta c^2] u_{k_i}^{(\sigma_i)}}{\omega_1^2 - (\mathbf{p}' + \mathbf{k}_i)^2 c^2 - c^4 + i\epsilon} \times F_L^c(p') F_L^c(|\mathbf{p}' + \mathbf{q}|) P_L(\cos \vartheta_{12}), \quad (2.19)$$

with $\cos \vartheta_{12} = \frac{1}{|\mathbf{p}' + \mathbf{q}|} [(k_f \cos \vartheta_f - k_i) \cos \vartheta_{p'} + k_f \sin \vartheta_{p'} \sin \vartheta_f \cos \varphi_{p'} - p']$, where ϑ_f is the scattering angle. The z axis is chosen along \mathbf{k}_i , and the (x, z) plane contains \mathbf{k}_f and hence \mathbf{q} . One has $F_L^c(q) \sim q^L$ for $q \rightarrow 0$, such that for $L \geq 1$ the integrand in (2.19) is well behaved and can be dealt with as described in [35].¹

The same integration variable \mathbf{p}' is chosen for the transverse term M_{fi}^{te1} , which relates to the second expression

in (2.4). With $q_1^2 = \Delta E_1/c^2 - \mathbf{q}_1^2 = (E_i - \omega_1)^2/c^2 - p^2$ and $\gamma_0 \gamma_m = \alpha_m$ one gets

$$M_{fi}^{te1}(L) = \frac{1}{2\pi^2 c} \int_0^\infty \frac{p'^2 dp'}{(E_i - \omega_1)^2/c^2 - p'^2 + i\epsilon} \int \frac{d\Omega_{p'}}{(\mathbf{p}' + \mathbf{q})^2} \times \sum_{m=1}^3 \frac{u_{k_f}^{(\sigma_f)+} [\omega_1 + c\boldsymbol{\alpha}(\mathbf{p}' + \mathbf{k}_i) + \beta c^2] \alpha_m u_{k_i}^{(\sigma_i)}}{\omega_1^2 - (\mathbf{p}' + \mathbf{k}_i)^2 c^2 - c^4 + i\epsilon} \times \sum_{M=-L}^L \left[T_{L,0m} - \hat{p}^m \sum_{k=1}^3 \hat{p}^k T_{L,0k} \right]. \quad (2.20)$$

For the transverse term M_{fi}^{te2} , relating to the third expression in (2.4), the choice $\mathbf{p}' = \mathbf{p} - \mathbf{k}_f = \mathbf{q}_2$ has to be made, such that $\mathbf{q}_1 = \mathbf{q} - \mathbf{p}'$. Then

$$M_{fi}^{te2}(L) = \frac{1}{2\pi^2 c} \int \frac{d\mathbf{p}'}{(\mathbf{q} - \mathbf{p}')^2} \frac{1}{\Delta E_2/c^2 - p'^2 + i\epsilon} \times \sum_{m=1}^3 \frac{u_{k_f}^{(\sigma_f)+} \alpha_m [\omega_1 + c\boldsymbol{\alpha}(\mathbf{p}' + \mathbf{k}_f) + \beta c^2] u_{k_i}^{(\sigma_i)}}{\omega_1^2 - (\mathbf{p}' + \mathbf{k}_f)^2 c^2 - c^4 + i\epsilon} \times \sum_{M=-L}^L \left[T_{L,m0} - \hat{p}^m \sum_{k=1}^3 \hat{p}^k T_{L,k0} \right], \quad (2.21)$$

where $\omega_1 = E_i - \omega_L + M_T c^2 - \sqrt{(\mathbf{q} - \mathbf{p}')^2 c^2 + M_T^2 c^4}$ and $\Delta E_2 = (\omega_1 - E_f)^2$.

The integration variable $\mathbf{p}' = \mathbf{q}_2$ for the third transverse term M_{fi}^{te3} from (2.5) is taken to be the same as for the second term, leading to identical expressions for \mathbf{q}_1 and ω_1 as in (2.21). One gets

$$M_{fi}^{te3}(L) = -\frac{1}{2\pi^2 c} \int \frac{d\mathbf{p}'}{(\mathbf{q} - \mathbf{p}')^2 - \frac{\Delta E_1}{c^2} - i\epsilon} \frac{1}{\frac{\Delta E_2}{c^2} - p'^2 + i\epsilon} \times \sum_{r,k=1}^3 \frac{u_{k_f}^{(\sigma_f)+} \alpha_r [\omega_1 + c\boldsymbol{\alpha}(\mathbf{p}' + \mathbf{k}_f) + \beta c^2] \alpha_k u_{k_i}^{(\sigma_i)}}{\omega_1^2 - (\mathbf{p}' + \mathbf{k}_f)^2 c^2 - c^4 + i\epsilon} \times \sum_{M=-L}^L \left[T_{L,rk} - \hat{q}_1^k \sum_{m=1}^3 \hat{q}_1^m T_{L,rm} - \hat{p}^r \sum_{m=1}^3 \hat{p}^m T_{L,mk} + \hat{p}^r \hat{q}_1^k \sum_{m=1}^3 \hat{q}_1^m \sum_{t=1}^3 \hat{p}^t T_{L,tm} \right], \quad (2.22)$$

with $\Delta E_1 = (E_i - \omega_1)^2$.

III. NUMERICAL INGREDIENTS

For the determination of the phase shifts, the electronic scattering states have to be calculated. They are obtained by means of solving the Dirac equation with the help of the Fortran code RADIAL of Salvat *et al.* [36]. The nuclear potential is generated from the Fourier-Bessel representation of the ground-state charge density of the ^{12}C nucleus [37].

¹In Eq. (2.19) of that work, the prefactor $2\sqrt{E_i E_f}/c^2$ is missing.

The phase-shift summation, required for the evaluation of the scattering amplitude f_{coul} [31], is performed with the help of a threefold convergence acceleration [38].

From the transition densities Q_L , $J_{L,L+1}$, and $J_{L,L-1}$ (note that in contrast to excitation by inelastic scattering, no weight factor $\sqrt{4\pi}$ is attached to the transition densities), the respective form factors are calculated. With the properties $F_L^c(q) \sim q^L$ and $F_{L\lambda}^{te}(q) \sim q^\lambda$ for $q \rightarrow 0$, and with their product entering into the integrals (2.20) and (2.21) by means of (2.9), the worst case for convergence, $\lambda = 0$, is unproblematic with the present choice of integration variables. M_{fi}^{te3} needs special care but is also convergent.

As for the first transverse term (2.20), its difference to the Friar-Rosen-type term (2.19) lies in the appearance of an additional pole p'_0 from the denominator $\Delta E_1/c^2 - p'^2 + i\epsilon$, where $p'_0 \approx \omega_L/c$. Writing the denominator from the electron propagator (2.2) in the form $F - G \cos \vartheta_{p'} + i\epsilon$ with ω_1 as defined above (2.19), the pathological solutions p'_1, p'_2 (with $p'_1 < p'_2$) from $F = -G$ can be determined analytically (avoiding Newton's method), and one finds nearly coincidence, $p'_1 \approx p'_0$. After extracting the singularity $\cos \vartheta_{p'} = F/G$ in the $\cos \vartheta_{p'}$ integral (see [35]) one is left with an integral of the type (with $\epsilon_0 \rightarrow 0$)

$$\begin{aligned} & \left(\int_{\alpha}^{p'_1 - \epsilon_0} + \int_{p'_1 + \epsilon_0}^{\beta} \right) dp' \frac{\ln |p'_1 - p'|}{p' - p'_0 - i\epsilon} f(p') \\ & \approx \left(\int_{\alpha}^{p'_1 - \epsilon_0} + \int_{p'_1 + \epsilon_0}^{\beta} \right) dp' \frac{\ln |p'_1 - p'|}{p' - p'_1 - i\epsilon} [f(p') - f(p'_1)] \\ & + f(p'_1) \left[-\frac{1}{2} \ln^2(p'_1 - \alpha) + \frac{1}{2} \ln^2(\beta - p'_1) + i\pi \ln |p'_0 - p'_1| \right], \end{aligned} \quad (3.1)$$

where $p'_0 = p'_1$ is used, except in the last term. Note that the p' -integration interval has not only to be split in p'_1 and p'_2 , but also in $|q|$.

The second transverse term (2.21) is much harder, and it is resorted to the approximation $\omega_1 \approx E_i - \omega_L$ (corresponding to $M_T \rightarrow \infty$), such that the pole p'_0 from $q_2^2 = 0$ remains angle independent and the further singularities attain a simple analytic form. Then the integrand has the structure

$$\begin{aligned} & \int_{\alpha}^{\beta} dp' \frac{p'^2}{p'^2 - p_0'^2 - i\epsilon} \int_{-1}^1 dx \\ & \times \int_0^{2\pi} d\varphi_{p'} \frac{1}{D - E \cos \varphi_{p'} + i\epsilon} \frac{1}{A + B \cos \varphi_{p'}} f(\mathbf{p}'), \end{aligned} \quad (3.2)$$

where $f(\mathbf{p}')$ is a well-behaved function, $x = \cos \vartheta_{p'}$, and the denominator $A + B \cos \varphi_{p'}$ results from $(\mathbf{q} - \mathbf{p}')^2$. It is unproblematic if $p' = |q|$ is avoided. The denominator $D - E \cos \varphi_{p'} + i\epsilon$ from the electron propagator depends now both on $\vartheta_{p'}$ and $\varphi_{p'}$. The pathological solutions $x_1(p')$, $x_2(p')$ from $|D| = E$ coincide for $p'_1 = |\sqrt{(E_i - \omega_L)^2/c^2 - c^2} - |\mathbf{k}_f||$ and $p'_2 = \sqrt{(E_i - \omega_L)^2/c^2 - c^2} + |\mathbf{k}_f|$, again with $p'_1 \approx p'_0$ close to ω_L/c . One can show that for $p' = p'_1$ and $p' = p'_2$ one has $x_1 = x_2 = -\cos \vartheta_f$, and $-1 \lesssim x_1 < x_2 < 1$ if $p'_1 < p' < p'_2$. The extraction of the singularities requires the following

integral:

$$\int_0^{\pi} d\varphi_{p'} \frac{1}{D - E \cos \varphi_{p'} + i\epsilon} = \frac{\pi \operatorname{sign}(D)}{\sqrt{(D + i\epsilon)^2 - E^2}}. \quad (3.3)$$

It is advantageous to split the x integral not only in x_1 and x_2 , but also in $\bar{x} = (x_1 + x_2)/2$. With the help of the formula

$$\begin{aligned} & \int dx \frac{1}{\sqrt{\alpha x^2 + 2\beta x + \gamma}} \\ & = \frac{1}{\sqrt{\alpha}} \left[\ln \left(\sqrt{\alpha} \sqrt{\alpha x^2 + 2\beta x + \gamma} + \alpha x + \beta \right) + \ln 2 \right], \end{aligned} \quad (3.4)$$

for $\alpha > 0$ one has, for example, after extraction of the singularities in the x integral, if $D(x = -1) < 0$,

$$\begin{aligned} & \int_{-1}^{\bar{x}} dx \frac{1}{\sqrt{(D + i\epsilon)^2 - E^2}} = \frac{1}{2p'|\mathbf{k}_f|c^2} \\ & \times \left[\ln \frac{\sin \vartheta_f}{1 + \cos \vartheta_f} + \frac{1}{2} \ln \frac{(p' + p'_2)(p' + p'_1)}{(p'_2 - p')(p' - p'_1)} + i \frac{\pi}{2} \right], \end{aligned} \quad (3.5)$$

valid for $p'_1 < p' < p'_2$. For $D(x = -1) \geq 0$, the sign of the last two terms is reversed, and the denominator in the first term turns into $1 - \cos \vartheta_f$. Thereby logarithmic singularities in p'_1 and p'_2 are produced such that an integral of type (3.1) is also needed here.

The integrand of the third transverse term (2.22) is identical to the one given in (3.2), except for the replacement of A by $A' = A - \omega_L^2/c^2$, adding $-i\epsilon$. However, the singularities from $A' + B \cos \varphi_{p'} = 0$ are no longer reduced in strength by the numerator, such that they have to be extracted in a similar way as those from $D - E \cos \varphi_{p'} = 0$. The pathological solutions $x'_1(p')$, $x'_2(p')$ from $|A'| = B$ coincide for $p'_3 = q - \omega_L/c$ and $p'_4 = q + \omega_L/c$. If one restricts the momentum transfer such that $1.5 p'_1 < p'_3 < q < p'_4 < 0.9 p'_2$, which covers the examples given below, the interval (p'_3, p'_4) lies completely inside (p'_1, p'_2) . Thus for $p' \in (p'_3, p'_4)$ the x -integration interval contains four singularities. For the points $p' \in \{p'_3, p'_4\}$ one has $x'_1 = x'_2 = (k_i - k_f \cos \vartheta_f)/q$, and the pathological intervals $[x_1, x_2]$ and $[x'_1, x'_2]$ where the $\varphi_{p'}$ integrand becomes singular are disjoint, $-1 < x_1 \leq x_2 < x'_1 \leq x'_2 < 1$. This allows for a separate treatment of the singularities of the two photon propagators.

While for the p' intervals $0 < p' < p'_3$ and $p'_4 < p' \leq p'_{\max}$ (with $p'_{\max} \approx 1.5 p'_2$), the same techniques are used as for M_{fi}^{te2} (merely substituting A' for A and using logarithmic integration steps near p'_3 and p'_4), the interval $p'_3 < p' < p'_4$ requires the following treatment. Defining the separation point $\bar{x}_0 = (x_2 + x'_1)/2$, the integral is split into two parts, $I_1 + I_2$,

$$\begin{aligned} & \int_{p'_3 + \epsilon_0}^{p'_4 - \epsilon_0} dp' \int_{-1}^1 dx f(p', x) = \int_{p'_3 + \epsilon_0}^{p'_4 - \epsilon_0} dp' \int_{-1}^{\bar{x}_0} dx f(p', x) \\ & + \int_{p'_3 + \epsilon_0}^{p'_4 - \epsilon_0} dp' \int_{\bar{x}_0}^1 dx f(p', x). \end{aligned} \quad (3.6)$$

In I_1 , the $\varphi_{p'}$ singularity is extracted with the help of the integral (3.3), whereas in I_2 , the two denominators of (3.2) are

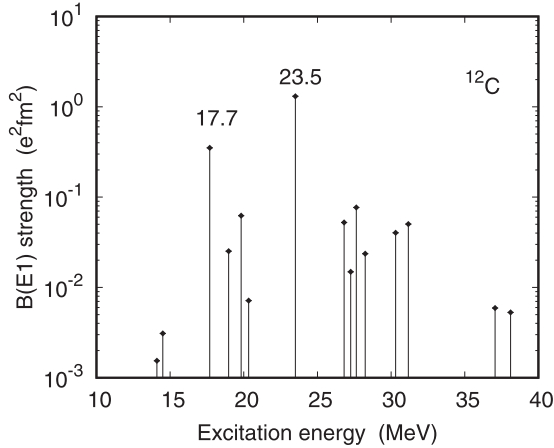


FIG. 3. Transition strength $B(E1)\uparrow$ for dipole excitation by means of an electromagnetic interaction with the ^{12}C nucleus as a function of excitation energy ω_L up to 40 MeV, calculated within the QRPA model [16].

interchanged. Thus an equation of type (3.3) comes into play, with $D + i\epsilon$ and E replaced by $A' - i\epsilon$ and B , respectively.

We note that in the intervals $-1 < x < x_1$ and $x_2 < x \leq \bar{x}_0$, the $\varphi_{p'}$ integrand is sharply peaked in $\cos \varphi_{p'} = \text{sign } D/E(x_2) = -1$, so that this value is extracted even if it is not a pole. A similar procedure is applied in the intervals $\bar{x}_0 \leq x < x'_1$ and $x'_2 < x < 1$. In the remaining intervals the true poles at $\cos \varphi_{p'} = D/E$, respectively, at $\cos \varphi_{p'} = -A'/B$, are used instead. A second extraction of the singularities from the remainder [i.e., from the right-hand side of (3.3)] is not done here. Logarithmic integration steps and a somewhat larger step number are sufficient. We estimate the numerical accuracy of the dispersion correction to be about 5%.

IV. RESULTS

We will first consider some properties of nuclear excitation and subsequently discuss the influence of transient excited states on the elastic scattering cross section. Thereby it is distinguished between the relative cross-section changes induced by Coulombic and magnetic transitions.

A. Transition to excited states

At collision energies near 200 MeV and beyond, the impinging electron will rather excite the nucleus than scatter elastically (except at small scattering angles). In the context of dispersion, dipole excitations are particularly important. In fact, the average value of the excitation energy, $\bar{\omega} = 15$ MeV, predicted by Friar and Rosen [9] for the use in the closure approximation, lies in the giant-dipole resonance region. Figure 3 shows the BE1 strength of the one-phonon 1^- states with excitation energies in the region between 10 and 40 MeV, as calculated by Ponomarev within the QRPA model [16]. For details see, e.g., Ref. [15]. This strength is related to the charge transition density for natural parity states, $\pi = (-1)^L$, by [29]

$$B(EL, 0^+ \rightarrow L^\pi) = (2L + 1) \left| \int_0^\infty r_N^{L+2} dr_N \varrho_L(r_N) \right|^2. \quad (4.1)$$

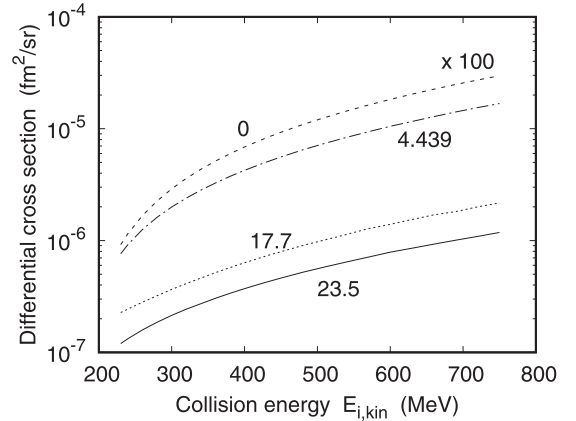


FIG. 4. Differential cross section $d\sigma/d\Omega_f$ in the first diffraction minimum of $d\sigma^{\text{Coul}}/d\Omega_f$ for the excitation of the 4.439-MeV ($L = 2$) state (— · — · —), the 17.7-MeV ($L = 1$) state (· · · · ·), and the 23.5-MeV ($L = 1$) state (——) as a function of collision energy $E_{i,\text{kin}}$. Included is the elastic Coulombic cross section $d\sigma^{\text{Coul}}/d\Omega_f$, multiplied by a factor of 100 (— · — · —).

There exist two particularly strong excitations, at 23.5 and 17.7 MeV, which will subsequently be used in the sum over n in (2.1).

In addition to the dipole excitations, there is a well-isolated 2^+ state at 4.439 MeV, which is the lowest quadrupole excitation in ^{12}C , with strength $B(E2, 0^+ \rightarrow 2^+) = 39.7 e^2 \text{fm}^4$ [39]. This state will also be included in the sum over n . Its transition densities are again calculated within the QRPA prescription and are provided in [40]. Figure 4 displays the electron-impact excitation cross section for these three states, calculated from the transition densities within the distorted-wave Born approximation (DWBA) [30,41]. For each collision energy, the cross sections are evaluated at the scattering angle corresponding to the first diffraction minimum according to Fig. 2(a). The quadrupole state with the lowest ω_L is the dominant one, while the 23.5-MeV dipole state is about a factor of 2 weaker than the 17.7-MeV state. Included is the elastic scattering result $d\sigma^{\text{Coul}}/d\Omega_f$, which in the figure is enhanced by a factor of 100. Beyond 400-MeV collision energy, the energy dependence of all processes, elastic and inelastic, is very similar.

In contrast to the elaborate DWBA calculation for excitation, the second-order Born theory, used for dispersion, requires form factors instead of transition densities. They are displayed in Fig. 5 for the three states under consideration. Note that the sign of $J_{L,L-1}$ has been reversed according to the convention of [29]. From Fig. 5(a) it follows that the charge form factors of the 23.5-MeV dipole state and the quadrupole state are of the same order of magnitude, while the one for the 17.7-MeV state is much smaller. In contrast, the magnetic form factor $F_{L,L+1}^{te}$ [Fig. 5(b)] is considerably stronger for the 17.7-MeV excitation. For the quadrupole state not only $F_{L,L+1}^{te}$ but also $F_{L,L-1}^{te}$ [Fig. 5(c)] is extremely weak.

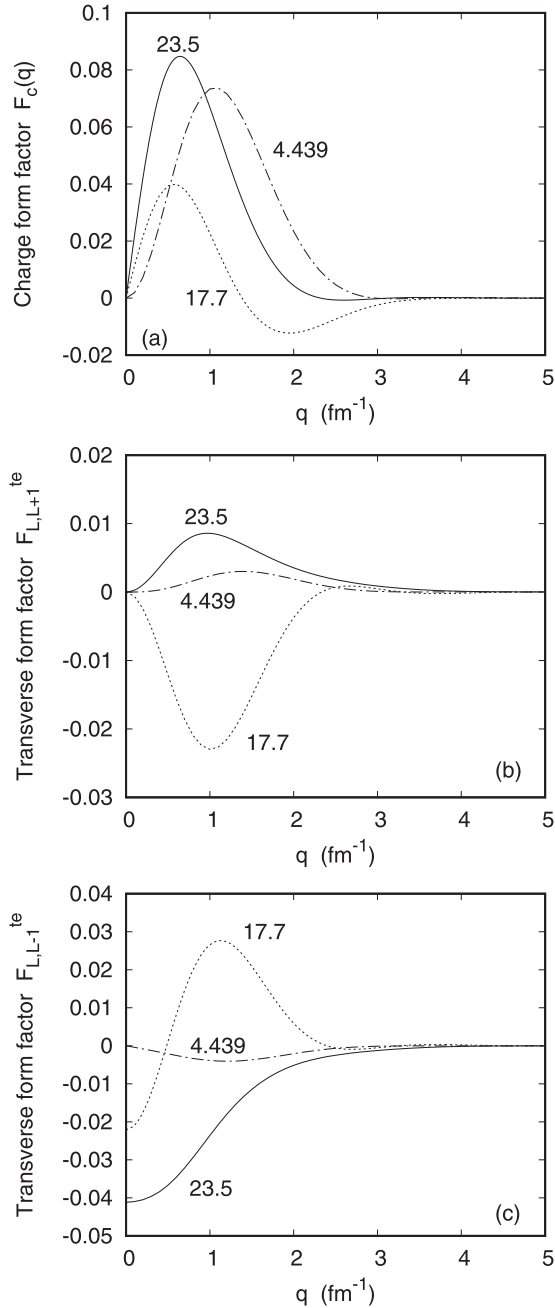


FIG. 5. Form factors for dipole and quadrupole excitation by electron impact on ^{12}C as a function of momentum transfer $|q|$. Shown are the results for the 23.5-MeV state (—), the 17.7-MeV state (⋯⋯⋯), and the 4.439-MeV state (— · — · —). (a) Charge form factor $F_c(|q|)$, (b) transverse form factor $F_{L,L+1}^{te}(|q|)$, and (c) transverse form factor $F_{L,L-1}^{te}(|q|)$.

B. Coulombic dispersion correction

Given the cross section (2.14) with the complete sum (2.15), the total dispersion correction $\Delta\sigma_{\text{box}}$ to the elastic scattering cross section from the phase-shift analysis is defined by

$$\Delta\sigma_{\text{box}} = \frac{d\sigma^{\text{box}}/d\Omega_f}{d\sigma^{\text{coul}}/d\Omega_f} - 1. \quad (4.2)$$

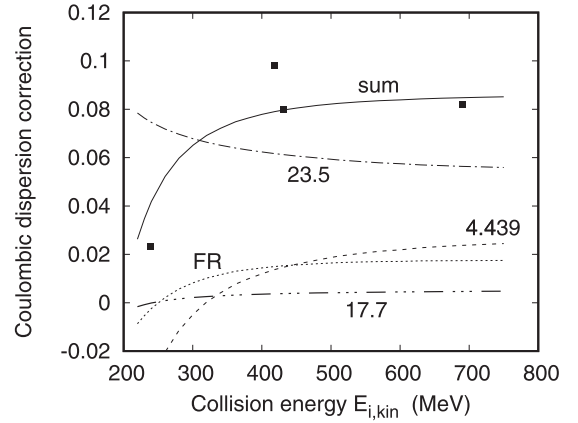


FIG. 6. Coulombic dispersion correction at the position of the first diffraction minimum of $d\sigma^{\text{coul}}/d\Omega_f$ as a function of collision energy. Shown is $\Delta\sigma_{\text{box}}$ from (4.2) (—) as well as its contributions from the transient 23.5-MeV state (— · — · —), from the 17.7-MeV state (⋯⋯⋯), and from the 4.439-MeV state (— · — · —). The Friar-Rosen result (with $\bar{\omega} = 15$ MeV) is included (⋯⋯⋯ [23]). The experimental data (■) are from Offermann and co-workers [3,4].

In order to distinguish the contributions $\Delta\sigma_{\text{box}}(L)$ from each excited state, characterized by the angular momentum L and the energy ω_L , the sum over L in (2.15) is dropped when inserting (2.14) into (4.2). Since these contributions add incoherently due to their linear entry into the cross section, the total dispersion correction can be written as

$$\Delta\sigma_{\text{box}} = \sum_L \Delta\sigma_{\text{box}}(L). \quad (4.3)$$

Note that the contributing states may have the same L but different ω_L .

In order to compare with the Friar-Rosen theory, one concentrates first on the Coulombic excitation of the transient nuclear states, that is, retaining only M_{fi}^c in (2.15) while setting the transverse terms equal to zero.

We resort again to the minimum position from Fig. 2(a), in the vicinity of which the dispersion effect is expected to be largest [11], to demonstrate the dependence on the collision energy. Figure 6 shows the contribution of the three selected states to $\Delta\sigma_{\text{box}}$. It is seen that at all energies the highest dipole state provides the largest portion of dispersion, mostly near 6%. In contrast, the quadrupole state furnishes at most 2%, which is of the order of the Friar-Rosen result. However, it compensates the decrease of the 23.5-MeV-state dispersion effect with energy. The contribution from the dipole state at 17.7 MeV is very small (below 0.5%).

A notable feature is the leveling of the dispersion correction beyond 400 MeV. It is related to the fact that the excitation probability of the three states increases with E_i in a similar way as the elastic process for such high energies (see Fig. 4) such that the quotient (4.2) tends to a constant. Also shown is the comparison of $\Delta\sigma_{\text{box}}$ with the experimental data from Offermann and co-workers [3,4], which result from high-precision measurements. Radiative corrections are already considered in the data. It is seen that the agreement with the measurements is greatly improved as compared to

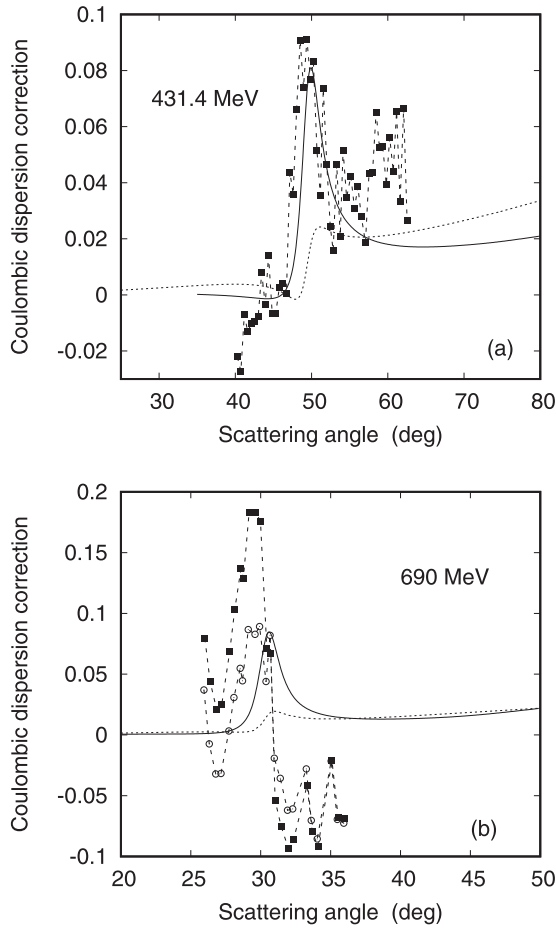


FIG. 7. Coulombic dispersion correction $\Delta\sigma_{\text{box}}$ (—) as a function of scattering angle ϑ_f (a) at an impact energy of 431.4 MeV and (b) at 690 MeV. Included is the result from the Friar-Rosen theory (····· [23]). The data points (■) in (a) are derived from the experimental cross sections of Offermann *et al.* [4]. In (b) the data points (■) are those from Kalantar-Nayestanaki *et al.* [3], and the other data points (○) result from a reevaluation of the measurements as described in the text. The dashed lines connect the experimental points as a guide to the eye. The oscillations at the larger angles are interpreted as experimental fluctuations.

the Friar-Rosen theory, where closure with $\bar{\omega} = 15$ MeV is used [23].

The angular dependence of the dispersion correction for two impact energies is shown in Fig. 7 in comparison with experiment and with the Friar-Rosen theory. For the collision energy of 431.4 MeV [Fig. 7(a)], the maximum value of $\Delta\sigma_{\text{box}}$ agrees with the data but is shifted to a slightly larger angle. The Friar-Rosen theory is far too low at the maximum; however, it reproduces the experimental increase of $\Delta\sigma_{\text{box}}$ for $\vartheta_f \gtrsim 55^\circ$, while the present theory is inferior in this respect. Noting that only the $L = 2$ intermediate state leads to an increase with angle, in contrast to the $L = 1$ states (see Fig. 8 below), this deficiency might result from the omission of excited states with higher multipolarity.

Figure 7(b) provides the results for $\Delta\sigma_{\text{box}}$ at a higher energy, 690 MeV. In accord with Fig. 6, its maximum is around

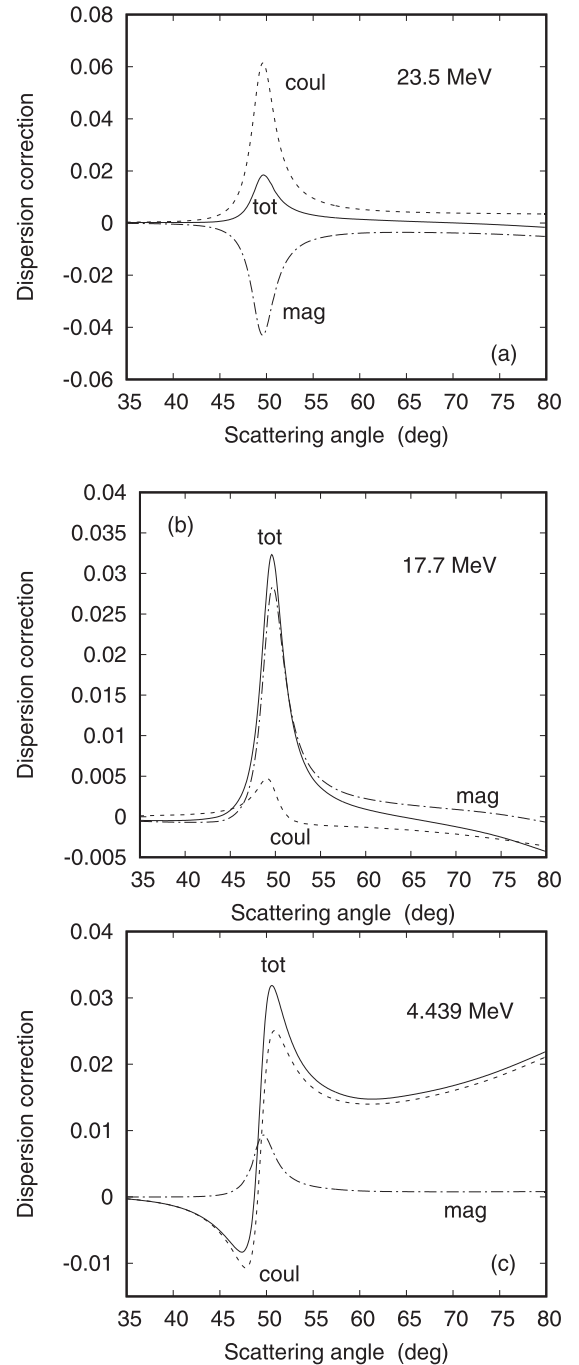


FIG. 8. Dispersion correction $\Delta\sigma_{\text{box}}(L)$ from 431.4-MeV $e + {}^{12}\text{C}$ collisions as a function of scattering angle ϑ_f : (a) for the transient excited $L = 1$ state at $\omega_L = 23.5$ MeV, (b) for the $L = 1$ state at $\omega_L = 17.7$ MeV, and (c) for the $L = 2$ state at $\omega_L = 4.439$ MeV. Shown are results from the Coulombic excitation (---), the magnetic excitation (- · - · -), and their sum (—).

8%. For this collision energy, no explicit cross-section data are available but only the reduced ones, according to (4.2), which depend on the theoretical estimates of [3] for the elastic cross section, and which are shown as black dots in the figure. These data imply a dispersion correction in the maximum, which is about a factor of 2 higher than our predictions, followed

by a very deep minimum at angles beyond the diffraction minimum.

This feature supports the suspicion that in the data reduction recoil was not treated properly. We performed a reevaluation of experiment in the following way. First to each value of the effective momentum transfer q_{eff} (the abscissa in the plot of [3]) the corresponding momentum transfer $|q|$ was associated, using the fact that the measurements extended from 26° to 36° . This led to a linear relation between q_{eff} and the pertinent scattering angle ϑ_f . Next $d\sigma^{\text{coul}}/d\Omega_f$ was calculated at each such angle ϑ_f , and by inversion of (4.2) the cross section $d\sigma_{\text{exp}}/d\Omega_f(\vartheta_f)$ was reconstructed. Looking at the angular dependence of these so-obtained experimental cross-section data in comparison with $d\sigma^{\text{coul}}/d\Omega_f$, a distinct shift of the experimental low-angle wing by $+0.06^\circ$ was discovered. (This is slightly lower than the calculated recoil-induced shift of $+0.10^\circ$.) To bring the two curves into agreement, each datum point at ϑ_f was now associated with the angle $\vartheta_f - 0.06^\circ$, and comparison was made with $d\sigma^{\text{coul}}/d\Omega_f(\vartheta_f - 0.06^\circ)$ to obtain $\Delta\sigma_{\text{box}}^{\text{exp}}$ via (4.2). This procedure results in the open circles shown in Fig. 7(b), the maximum of which is now in reasonable agreement with the maximum of $\Delta\sigma_{\text{box}}$. Only the mismatch of its angular position is somewhat larger than at the lower energy. We note that the 690-MeV data points in Figs. 2 and 6 were obtained from these reevaluated data.

C. Magnetic contribution

Magnetic transitions can play an important role in excitation by electron impact. For the collision energy of 431.4 MeV and an angle of 49° ($q = 1.8 \text{ fm}^{-1}$), magnetic scattering contributes, respectively, 29%, 52%, and 1% to the cross sections for the $L = 1$ (23.5 MeV), $L = 1$ (17.7 MeV), and $L = 2$ (4.439 MeV) excitations. Therefore a similar influence on $\Delta\sigma_{\text{box}}$ will occur, maybe even somewhat enhanced by the presence of three magnetic terms (instead of one in excitation).

The effect of magnetic scattering on the dispersion-corrected cross section is obtained from (2.14) by setting $M_{fi}^c = 0$ in (2.15). We note that for the highly relativistic systems considered here, M_{fi}^{te1} , M_{fi}^{te2} , and M_{fi}^{te3} can be of comparable magnitude. In such a case, M_{fi}^{te2} and M_{fi}^{te3} tend to compensate each other.

For each of the three transient excited states, the Coulombic and magnetic contribution to dispersion are displayed separately in Fig. 8. For the $L = 1$ state at 23.5 MeV [Fig. 8(a)], the transition currents tend to compensate the influence of the transition charge density, such that the total dispersion effect is below 2%. In case of the lower-energy $L = 1$ state [Fig. 8(b)], the dispersion correction results nearly exclusively from magnetic scattering, while the $L = 2$ state [Fig. 8(c)] shows the opposite behavior.

Whereas magnetic scattering is far from negligible for the $L = 1$ excited states, the total dispersion correction from including the three states is very similar to the dispersion from Coulombic excitation alone. This is demonstrated in Fig. 9(a) for 431.4-MeV impact along with the experimental data from Fig. 7(a). In fact, the total dispersion correction deviates no-

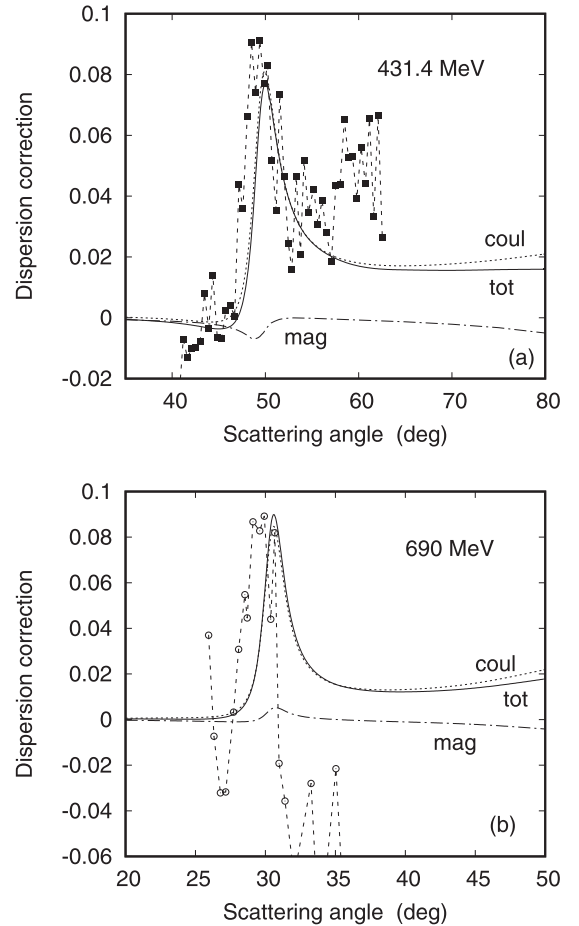


FIG. 9. Dispersion correction $\Delta\sigma_{\text{box}}$ from (a) 431.4 MeV and (b) 690 MeV $e + {}^{12}\text{C}$ collisions as a function of the scattering angle. Shown is the Coulombic contribution from Fig. 7 (.....), the magnetic contribution (— · — · —), and their sum (———). All results include the sum over L in (2.15). The data points are those from Fig. 7.

tably from the Coulombic correction only at scattering angles near 45° , in the peak maximum and above 65° .

Figure 9(b) shows the respective result at 690 MeV. Also for this higher energy the total dispersion correction is very similar to the Coulombic one, while the total magnetic scattering is small. For the individual transient states, as compared to Fig. 8, the magnetic contribution from the 23.5-MeV state is only half as large in the maximum as in case of the lower collision energy. For the other two excited states the situation is basically the same as shown in Figs. 8(b) and 8(c).

Figure 10(a) displays the situation in the first diffraction minimum. At energies below 400 MeV, the inclusion of magnetic scattering lowers the dispersion correction considerably and altogether leads to a stronger increase of $\Delta\sigma_{\text{box}}$ as the projectile gets faster. Figure 10(b) furnishes the total contribution from each of the excited states. The situation differs from the pure Coulombic case (Fig. 6) in that the 4.439-MeV state is nearly equally important as the 23.5-MeV state, which dominates the dispersion correction from the Coulombic excitation. At the lower energies, a large part of $\Delta\sigma_{\text{box}}$ results from the

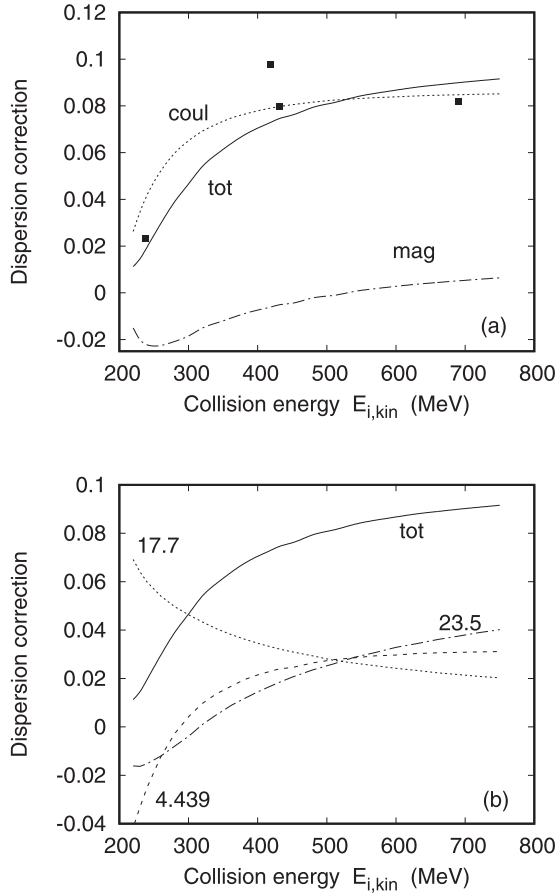


FIG. 10. Dispersion correction $\Delta\sigma_{\text{box}}$ at the position of the first diffraction minimum as a function of collision energy. Shown in (a) together with the experimental data from Offermann and co-workers (■ [3,4]) is the Coulombic part from Fig. 6 (.....), the magnetic contribution (---), as well as their sum (—). All three excited states ($L = 1, 2$) are taken into account. Shown in (b) is $\Delta\sigma_{\text{box}}$ when considering $\omega_L = 23.5$ MeV (---), 17.7 MeV (.....), and 4.439 MeV (— · — · —), as well as their sum (—). All four contributions to A_{fi}^{box} are taken into account.

17.7-MeV excitation, the Coulombic contribution to which is completely unimportant.

V. CONCLUSION

We have estimated the influence of dispersion on the elastic scattering cross section from electron impact on a carbon nucleus. Since ^{12}C is a light nucleus, we are confident that the results from the second-order Born approximation for the box diagram, paired with the partial-wave analysis for elastic potential scattering, are reliable concerning the influence of Coulomb distortion effects. Compared to the standard theory of Friar and Rosen for ^{12}C , we have (i) dropped the closure approximation and instead explicitly considered the transient excitation to two prominent dipole and one low-lying quadrupole state by means of accurate form factors available

within the QRPA model. And (ii), we have included the magnetic part of the two photon propagators.

By accounting for the transient excitation of the three prominent states, we found an enhancement of the dispersion correction as compared to the Friar-Rosen predictions by a factor of 5 in its maximum region for energies above 300 MeV.

Considering the angular dependence of the dispersion effect at two sample impact energies, 431.4 and 690 MeV, where accurate experimental data are available, the experimental peak height is approximately reproduced (if a recoil-based reevaluation of the 690-MeV data is made), while the peak position is at too large an angle as compared to the measurements. Also there is some disagreement in the low- and high-energy wings. The angular distribution, predicted by the Coulombic excitation of the transient nuclear states, is only marginally changed when the magnetic terms are added.

As for the contribution of the individual excited states at both impact energies, it is found that the 23.5-MeV $L = 1$ state yields the dominant Coulombic part of $\Delta\sigma_{\text{box}}$, whereas the one from the 17.7-MeV $L = 1$ state is negligible. However, considering both Coulombic and magnetic contributions, the 4.439-MeV $L = 2$ and the 17.7-MeV states have equal shares in the maximum for 431.4-MeV impact, the quadrupole state taking over at angles beyond the peak. The 23.5-MeV state furnishes only 2% to $\Delta\sigma_{\text{box}}$ in the maximum. At 690 MeV, the contribution of the 23.5-MeV state in the maximum has increased to nearly 4%.

In order to systematically investigate the dependence of dispersion on collision energy from 220 to 750 MeV, we have studied the cross-section change in the first diffraction minimum of the elastic cross section where it is largest. In this geometry, the addition of the magnetic scattering leads to a steeper increase of $\Delta\sigma_{\text{box}}$ with energy, yielding up to 9% at the highest energies. For the slower collisions, the 17.7-MeV state provides the dominant contribution, its effect being partially canceled by the consideration of the 4.439-MeV state. Near 500 MeV, all three transient states contribute equally, while at still larger energies the highest excited state considered takes over. As compared to the mere Coulombic excitation, the basic effect of magnetic scattering is a decrease of $\Delta\sigma_{\text{box}}$ by 30%–70% at energies below 300 MeV.

To conclude, magnetic scattering plays a decisive role for dispersion in contrast to early conjectures about its irrelevance. Although the considered high-energy intermediate dipole states together with the strong low-lying quadrupole excitation give a qualitative prescription of the dispersion correction to the differential cross section, the influence of transient nuclear states of higher multipolarity is still an open question. Also, at energies well beyond 400 MeV the excitation of baryon resonances and intermediate-state pions, not considered in the QRPA model for the transition densities, may have some influence on dispersion. Further experimental and theoretical investigations are needed to clarify this point.

ACKNOWLEDGMENTS

I would like to thank A. V. Afanasev for stimulating this project and for fruitful comments. I am particularly grateful

to V. Yu. Ponomarev for calculating the dipole transition densities and the B(E1) strength distribution. I would also

like to thank P. A. Amundsen for his help with a technical detail.

-
- [1] I. Sick and J. Mc Carthy, *Nucl. Phys. A* **150**, 631 (1970).
- [2] W. Reuter, G. Fricke, K. Merle, and H. Miska, *Phys. Rev. C* **26**, 806 (1982).
- [3] N. Kalantar-Nayestanaki, C. W. de Jager, E. A. J. M. Offermann, H. de Vries, L. S. Cardman, H. J. Emrich, F. W. Hersman, H. Miska, and D. Rychel, *Phys. Rev. Lett.* **63**, 2032 (1989).
- [4] E. A. J. M. Offermann, L. S. Cardman, C. W. de Jager, H. Miska, C. de Vries, and H. de Vries, *Phys. Rev. C* **44**, 1096 (1991).
- [5] P. Guèye *et al.* (Jefferson Lab Hall A Collaboration), *Eur. Phys. J. A* **56**, 126 (2020).
- [6] L. I. Schiff, *Phys. Rev.* **98**, 756 (1955).
- [7] R. R. Lewis, *Phys. Rev.* **102**, 544 (1956).
- [8] J. L. Friar and M. Rosen, *Phys. Lett. B* **39**, 615 (1972).
- [9] J. L. Friar and M. Rosen, *Ann. Phys.* **87**, 289 (1974).
- [10] A. Bottino and G. Ciocchetti, *Nucl. Phys. A* **178**, 593 (1972).
- [11] T. De Forest, *Phys. Lett. B* **32**, 12 (1970).
- [12] A. Goldberg, *Il Nuovo Cimento* **20**, 1191 (1961).
- [13] A. Lovato, S. Gandolfi, J. Carlson, S. C. Pieper, and R. Schiavilla, *Phys. Rev. Lett.* **117**, 082501 (2016).
- [14] J. Goldemberg and R. H. Pratt, *Rev. Mod. Phys.* **38**, 311 (1966).
- [15] V. Yu. Ponomarev, D. H. Jakubassa-Amundsen, A. Richter, and J. Wambach, *Eur. Phys. J. A* **55**, 236 (2019).
- [16] V. Yu. Ponomarev (private communication).
- [17] V. G. Soloviev, *Theory of Atomic Nuclei: Quasiparticles and Phonons* (Institute of Physics, Bristol, 1992).
- [18] N. Lo. Iudice, V. Yu. Ponomarev, Ch. Stoyanov, A. V. Sushkov, and V. V. Voronov, *J. Phys. G: Nucl. Part. Phys.* **39**, 043101 (2012).
- [19] H. Bethe and A. Molinari, *Ann. Phys.* **63**, 393 (1971).
- [20] A. V. Afanasev and N. P. Merenkov, *Phys. Rev. D* **70**, 073002 (2004).
- [21] A. V. Afanasev and N. P. Merenkov, *Phys. Lett. B* **599**, 48 (2004); [arXiv:hep-ph/0407167v2](https://arxiv.org/abs/hep-ph/0407167v2) (2005).
- [22] L. C. Maximon and J. A. Tjon, *Phys. Rev. C* **62**, 054320 (2000).
- [23] D. H. Jakubassa-Amundsen, [arXiv:2102.08069](https://arxiv.org/abs/2102.08069) [nucl-th].
- [24] J. D. Bjorken and S. D. Drell, *Relativistic Quantum Mechanics* (McGraw-Hill, New York, 1964).
- [25] T. A. Griffy, D. S. Onley, J. T. Reynolds, and L. C. Biedenharn, *Phys. Rev.* **128**, 833 (1962).
- [26] D. G. Ravenhall and J. Wambach, *Nucl. Phys. A* **475**, 468 (1987).
- [27] H. C. Lee, Atomic Energy of Canada Report No. AECL-4839, Ontario, 1975.
- [28] A. R. Edmonds, *Angular Momentum in Quantum Mechanics*, 2nd ed. (Princeton University Press, Princeton, NJ, 1960).
- [29] J. Heisenberg and H. P. Blok, *Annu. Rev. Nucl. Part. Sci.* **33**, 569 (1983).
- [30] D. H. Jakubassa-Amundsen, *Nucl. Phys. A* **937**, 65 (2015).
- [31] V. B. Berestetskii, E. M. Lifshitz, and L. P. Pitaevskii, *Quantum Electrodynamics*, 2nd ed., Course of Theoretical Physics, Vol. 4 (Elsevier, Oxford, 1982).
- [32] N. T. Meister and T. A. Griffy, *Phys. Rev.* **133**, B1032 (1964).
- [33] L. C. Maximon, *Rev. Mod. Phys.* **41**, 193 (1969).
- [34] T. W. Donnelly and I. Sick, *Rev. Mod. Phys.* **56**, 461 (1984).
- [35] D. H. Jakubassa-Amundsen, *Eur. Phys. J. A* **57**, 22 (2021).
- [36] F. Salvat, J. M. Fernández-Varea, and W. Williamson, Jr., *Comput. Phys. Commun.* **90**, 151 (1995).
- [37] H. de Vries, C. W. de Jager, and C. de Vries, *At. Data Nucl. Data Tables* **36**, 495 (1987).
- [38] D. R. Yennie, D. G. Ravenhall, and R. N. Wilson, *Phys. Rev.* **95**, 500 (1954).
- [39] S. Raman, C. W. Nestor, Jr., and P. Tikkanen, *At. Data Nucl. Data Tables* **78**, 1 (2001).
- [40] D. H. Jakubassa-Amundsen and V. Yu. Ponomarev, *Eur. Phys. J. A* **56**, 162 (2020).
- [41] S. T. Tuan, L. E. Wright, and D. S. Onley, *Nucl. Instrum. Methods* **60**, 70 (1968).